ELSEVIER

Comput. Methods Appl. Mech. Engrg. 188 (2000) 17–38

Computer methods in applied mechanics and engineering

www.elsevier.com/locate/cma

Functionally graded material: a parametric study on thermal-stress characteristics using the Crank–Nicolson–Galerkin scheme

J.R. Cho [a,*], J. Tinsley Oden [b]

[a] *School of Mechanical Engineering, Pusan National University, San 30, Jangjeon-Dong, Kumjung-Ku, Pusan 609-735, South Korea*
[b] *Texas Institute for Computational and Applied Mathematics, The University of Texas at Austin, Austin, TX 78712, USA*

Received 13 July 1998; received in revised form 16 November 1998

Abstract

In this paper, we analyze thermal-stress characteristics of functionally graded materials (FGM), the newly introduced layered composite materials with great potential as next generation composites. Among the several material parameters governing its characteristics, we study the effects of the material variation through the thickness and the size of the FGM layer inserted between metal and ceramic layers using the finite element method. Through a representative model problem, we observe different thermal stress characteristics for different material variations and sizes of FGM. This basic study provides insight into the concept of FGM and lays the foundation of FGM optimization to control thermal stresses.

1. Introduction

Layered composite materials, due to their thermal and mechanical merits compared to single-composed materials, have been widely used for a variety of engineering applications. However, owing to the sharp discontinuity in the material properties at interfaces between two different materials, there may exist stress concentrations which result in severe material failure [25,32].

To remedy such defects, in 1989, the NKK Corporation in Japan initiated studies on functionally graded materials (FGM) [17,26]. At that time, applications to thermal-resistant structures of space shuttles were targeted [33]. However, recently, intensive and active research for various engineering applications have been under way in many countries [17].

As indicated from the term *functionally graded*, FGM has continuously varying material composition variation through the thickness such that it can satisfy the desired goals. The comparison between classical and FGM layered composites is illustrated in Fig. 1. Referring to Fig. 1, material composition is 100% metal at the interface between layers (1) and (3), while it becomes 100% ceramic at the interface between layers (2) and (3). Therefore, since there is no sharp discontinuity in material composition through the thickness, jumps in resulting thermal stresses are minimized. From the illustration, we see that FGM exhibits smoother thermal-stress distribution compared to classical layered composites (CLC).

In FGM, major concerns are the effects of the material composition variation and the relative thickness ratio of the FGM layer (3) inserted between metal and ceramic layers, because its thermal and mechanical behavior is significantly affected by these two parameters (for example, the maximum value and the

* Corresponding author.

0045-7825/00/$ - see front matter
PII: S0045-7825(99)00289-3

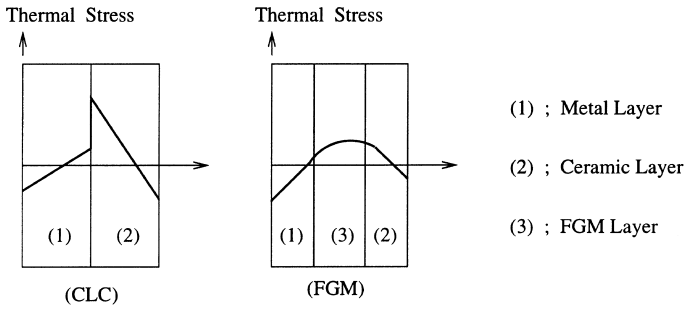

Fig. 1. Illustration of thermal characteristics between CLC and FGM composites.

smoothness of the thermal-stress distribution are different for different choices of the two parameters). In this study, we hierarchically investigate the effects of such parameters on thermomechanical characteristics for plane-stress two-dimensional Ni–Al_2O_3 FGMs subject to uniform heating through the numerical simulations using the finite element method.

2. Functionally graded materials

For the purpose of theoretical investigation, we consider a two-dimensional symmetric FGM beam, as shown in Fig. 2, where $2d$ and $2d_m$ represent, respectively, the thickness of the beam and the middle FGM layer. The coordinate z is directed upwards normal to the mid-surface of the beam. Throughout this paper, we indicate the entire FGM composite by FGM, while the inserted middle layer by the FGM layer. Furthermore, we assume that ceramic and metal layers are homogeneous and isotropic, and the FGM layer is inhomogeneous but macroscopically isotropic.

In this section, we hierarchically analyze the two parameters, and summarize the material-property variations through the thickness for the analysis in the following sections. Here, by the term *hierarchically* (or *hierarchical*) in this paper is meant that, by continuously varying a specific parameter, the corresponding behavior of FGMs, when measured along the specifically defined basis, shows sort of sequential variations (but, not monotonically). In this paper, with the basis defined in Section 2.1, we examine the thermal stresses with the two parameters, the variation of material composition and the relative size of the FGM layer.

2.1. Definition of two parameters

Referring to Fig. 3, we define the *composition volume fraction functions*, $V_c,\ V_m \in \mathscr{C}^0(-d,d)$ for ceramic and metal, respectively, such that

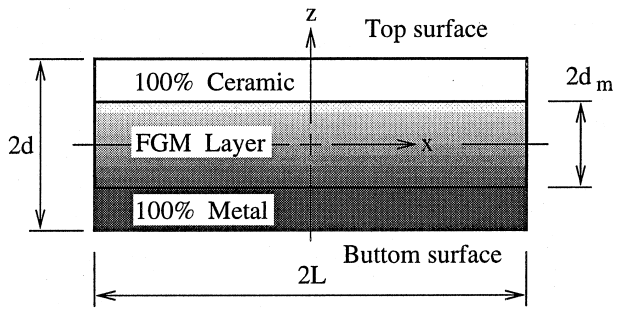

Fig. 2. A two-dimensional symmetric functionally graded composite beam.

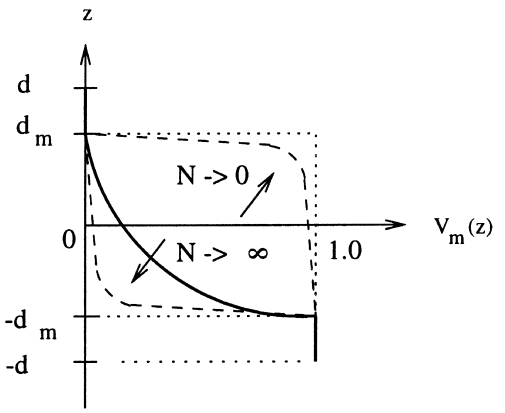

Fig. 3. Composition volume fraction of metal through the FGM thickness.

$$
\begin{aligned}
&V_{\mathrm{c}}(z) + V_{\mathrm{m}}(z) = 1, \quad V_{\mathrm{c}}(z) \leqslant 1, \quad |z| \leqslant d, \\
&V_{\mathrm{m}}(z) = \left[\frac{d_{\mathrm{m}} - z}{2d_{\mathrm{m}}}\right]^{N}, \quad |z| \leqslant d_{\mathrm{m}}, \\
&V_{\mathrm{m}}(z) = 1, \quad -d \leqslant z \leqslant -d_{\mathrm{m}}, \\
&V_{\mathrm{m}}(z) = 0, \quad d_{\mathrm{m}} \leqslant z \leqslant d,
\end{aligned}
\tag{1}
$$

where N are non-negative real numbers ($N \geqslant 0$). By changing the value of N, we can construct an infinite number of such functions. Here, the special cases are for $N \to 0$ and for $N \to \infty$, because these cases correspond to CLCs. We note that the former limit approaches the *metal layer-extended CLC* (m-CLC), while the latter limit approaches the *ceramic layer-extended CLC* (c-CLC), as depicted in Fig. 4. Next, referring to Fig. 2, we define the *relative thickness ratio* χ as

$$\chi = d_{\mathrm{m}}/d, \quad 0 \leqslant \chi \leqslant 1 \tag{2}$$

which is proportional to the relative region of the FGM layer with respect to the composite body. As χ tends to 0, FGMs approach CLCs, while they approach the *fully FGMs* (f-FGM) as $\chi \to 1$.

According to the two defined parameters, we can construct two different hierarchical families $\mathscr{F}_H^N$ and $\mathscr{F}_H^\chi$ for layered composites to examine the variations in thermal-stress characteristics. For the detailed mathematical abstraction and physical concept of hierarchical modeling, see [5] for isotropic elastic structures and [20] for heterogeneous elastic structures.

First, for a given power index N ($0 < N < +\infty$), the *χ-hierarchical family* $\mathscr{F}_H^\chi$ is defined as a set of infinite layered composite materials which are sequentially distinguished by the choice of relative thickness ratios χ such that

$$\mathscr{F}_H^\chi = \left\{ \mathscr{M}_N^\chi : \mathscr{M}_N^0 = \mathrm{CLC},\ \mathscr{M}_N^1 = \text{f-FGM},\ 0 \leqslant \chi \leqslant 1 \right\}. \tag{3}$$

Here, the lowest model is CLC and the highest model is the f-FGM.

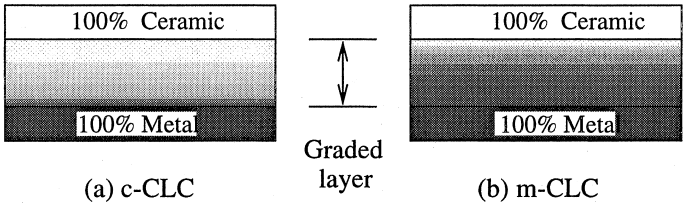

Fig. 4. Ceramic layer- and metal layer-extended classical layered composites: (a) c-CLC and (b) m-CLC.

Along the similar pattern to the definition of $\mathscr{F}_H^{\chi}$, the *N-hierarchical family* for a fixed relative thickness χ $(0 < \chi < 1)$ is defined as

$$\mathscr{F}_H^N = \left\{ \mathscr{M}_{\chi}^N : \mathscr{M}_{\chi}^0 = \text{m-CLC},\ \mathscr{M}_{\chi}^{\infty} = \text{c-CLC},\ 0 \leqslant N \leqslant \infty \right\}. \tag{4}$$

In particular, FGMs in this family approach m-CLCs as $N \to 0$ while they approach c-CLCs as $N \to \infty$. Therefore, in this family, the two lowest models are c- and m-CLCs, but the highest model is not clear.

The corresponding basis for the parametric investigation of the hierarchical families is defined in the following section dealing with the thermal-stress in FGMs.

2.2. Material properties of graded composites

In order to compute the temperature and the overall strain/stress distributions in FGMs, one needs the appropriate estimates for properties of the graded layer, such as the thermal conductivity, the coefficient of thermal expansion, the Young's modulus, Poisson's ratio and so on. A large number of papers on the thermomechanical response and the material properties of compositionally graded materials have been published, and they can be classified largely into theoretical and experimental categories. The progress in theoretical methods for the overall thermomechanical properties can be seen in a book by Christensen [7], and the discussion on experimental approaches in a paper by Suresh and coworkers (see e.g. [16]). In addition, the thermomechanical response by the theoretical approach can be modeled at microscopic (predicted upon the interaction between matrix and inclusions) and continuum levels (by accounting for only the volume fraction and individual properties of the constituent phases).

The prediction methods of the overall thermomechanical properties within the framework of single continuum mechanics are generally classified into three: (a) direct, (b) variational and (c) approximation approaches [28]. As is well described in a paper by Hill [13], the direct approach seeks the closed-form analytic solutions to the overall properties of ideal composites, wherein geometrical and other simplifications are made for mathematical derivation. As an alternative approach of rigorous mathematical treatment in the direct method, the variational approach provides the upper and lower bounds for the overall properties expressed in terms of the phase volume fraction [12]. Besides the bounded-form estimation, as described in [28], this approach does not specify the details in the phase geometry, one thus requires some reasonable approximations to obtain corresponding closed-form estimates.

In the approximation approach, the self-consistent models by Hill [14], Walpole [30] and Budiansky [3], the mean-field micromechanics models by Mori and Tanaka [18] and Wakashima and Tsukamoto [28,29], the modified rule of mixtures by Tamura and others (see e.g. [27]) and the unit cell model by Ravichandran [21] are representative homogenized (or averaging) estimates for the overall material properties. These averaging methods are simple and convenient to predict the overall thermomechanical response and properties, however, owing to the assumed simplifications, the validity in real FGMs is affected by the detailed microstructure and other conditions. We here briefly describe each of these together with its assessment by comparing with the *Hashin–Shtrikman*'s bounds, the experimental results and the detailed finite element analysis of the discrete models [9,22,23,31].

The self-consistent model is based on the *Eshelby*'s equivalent inclusion method, and have been reported to be generally suitable for relatively simple microstructures of low volume fractions. According to the work by Grujicic and Zhang [9] with the VCFEM (a Voronoi cell finite element method proposed orginally by Ghosh and Mukhopadhyay [11] for the calculation of material properties), the self-consistent method is not suitable for the FGMs of microstructures varying continuously, particularly consisting of interwined clusters of phases. Furthermore Dvorak and coworkers (see e.g. [22]) reported, from the numerical results obtained using the planar hexagonal-arrayed discrete model subjected to uniform and continuously varying traction/essential boundary conditions, that the self-consistent models are better for skeleton microstructures in a wide transition zone.

The Wakashima–Tsukamoto mean-field micromechanics model is to exploit the *Eshelby*'s equivalent inclusion method by incorporating the Mori–Tanaka concept [6,18] for the average (overall or regularized) stress, wherein the overall macromechanical properties $\bar{\boldsymbol{E}}$ are defined by

$$\langle\sigma\rangle_{\Omega} = \bar{\boldsymbol{E}} : \langle\varepsilon\rangle_{\Omega}, \tag{5}$$

$$\langle\cdot\rangle_{\Omega} = \frac{1}{|\Omega|}\int_{\Omega}\langle\cdot\rangle\,\mathrm{d}\Omega, \tag{6}$$

where, Ω denotes a representative volume element (RVE) [28,29]. Wakashima and Tsukamoto derived the expressions for the overall properties and presented the numerical results showing the comparison with the *Hashin–Shtrikman*'s bounds for two representative binary systems, the macroscopically isotropic particulate composite with randomly oriented and uniformly dispersed spheroidal particles, and the macroscopically transversely isotropic composite with unidirectionally continuous filaments of uniform cross section. We record the formula for the former case in Appendix A.

As is well established in [18,22], the Mori–Tanaka estimates are derived with randomly oriented and uniformly dispersed ellipsoidals in an infinite continuous matrix. Therefore the Mori–Tanaka and Wakashima–Tsukamoto estimates produce generally stiffer mechanical response [31], and further they become increasingly more inaccurate as a macrostructure tends to the microstructural size. In addition, they show good agreement with *Hashin–Shtrikman*'s bounds only when the difference in elastic moduli of two constituent phases is large, according to the work by Dvorak and coworkers [22,23].

For the Young's modulus of two-phase graded materials, Tamura and coworkers [27] proposed the modified rule of mixtures, which was subsequently adapted by Williamson et al. [32], Suresh and others [8,16] and so on. According to this approach, each sublayer in the graded layer is treated as an isotropic composite for which the uniaxial stress σ and strain ε are expressed in terms of the average uniaxial stress σ_i and ε_i (i denoted by each constituent phase) and the volume fraction such that

$$\sigma = \sigma_{\mathrm{A}}V_{\mathrm{A}} + \sigma_{\mathrm{B}}V_{\mathrm{B}}, \quad \varepsilon = \varepsilon_{\mathrm{A}}V_{\mathrm{A}} + \varepsilon_{\mathrm{B}}V_{\mathrm{B}} \tag{7}$$

together with the ratio of stress to strain transfer q given by

$$q = \frac{\sigma_{\mathrm{A}} - \sigma_{\mathrm{B}}}{\varepsilon_{\mathrm{A}} - \varepsilon_{\mathrm{B}}}. \tag{8}$$

Fig. 5(a) schematically illustrates this approach, and the value q is determined by experiments. The value q of 4.5 GPa chosen from the experiments has been justified by Suresh and coworkers [8,10,16]) and Williamson et al. [32] for the Ni–Al_2O_3 FGMs with a wide range of volume fraction and applied tractions.

Fig. 5(b) shows a schematic idea of the unit cell approximation proposed by Ravichandran [21]. In this approach, a two-phase composite is modeled by one with periodically located cubic cells. With this model, the formula for the Young's modulus and the Poisson's ratio of composites are derived. However, this method does not account for interaction between two phases by assuming perfect bonding. Additionally the Young's modulus is derived upon the assumption of the same Poisson's ratio for two phases. Assessment through the comparison with experimental data is addressed in [21], where the Young's modulus is reported to coincide with experimental data, but Poisson's ratio is not.

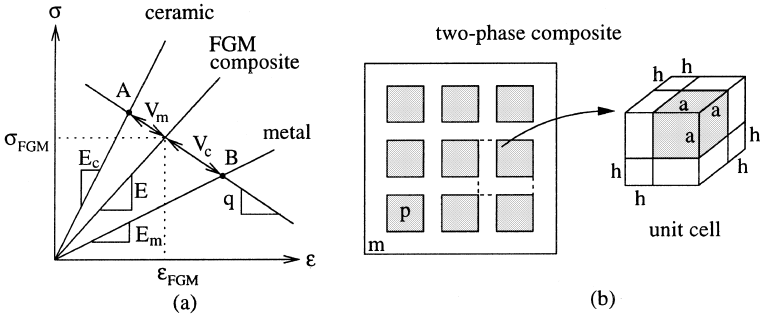

Fig. 5. Schematic representation of two averaging approaches for stress–strain data of FGMs: (a) the modified rule of mixtures and (b) the unit cell approximation.

Although the aforementioned single homogenized continuum models have been adequate for static and quasi-static problems, they lose completely any characterization in dynamical processes. This is because the single homogenized continuum model cannot capture dispersion and dissipation caused by structural effects in the dynamical process. The reader may refer to Bedford and Stern [1] and Bowen et al. [2] for the superimposed continua model which accounts for thermal and mechanical interactions.

As pointed out in the recent paper by Suresh and others [31], the averaging methods require more detailed analysis for the constituent phases of nonuniform geometries with sharp corners and for adequate capturing large fluctuations in microscopic thermomechanical fields and strain localization due to the non-uniform/non-periodic distributions of the constituent phases. However, referring to the recent work by Reiter and Dvorak [23] on the assessment of the homogenized methods by the detailed finite element analysis with the discrete model, the averaging methods may be selectively applied to FGMs subjected to both uniform and non-uniform overall loads with a reasonable degree of confidence.

According to comparison of the approaches discussed so far and the choice of metal and ceramic for our study, we employ the modified rule of mixtures for the Young's modulus of the graded layer. For the specific heat, the density, the thermal conductivity, the thermal expansion coefficient and Poisson's ratio, we simply use the linear rule of mixtures. For the dual-phase composite materials for which the difference in thermal expansion coefficients of two constituent phases is less than 1.0×10^{-7} K^{-1}, the justification of the linear rule of mixtures for the thermal expansion coefficient has been provided by Schapery [24].

3. Thermal stresses in FGM

For a mathematical characterization of thermal stresses in general FGMs, we consider a three-dimensional symmetric composite plate in which each layer is of uniform thickness, as shown in Fig. 6, where, Ω is an open bounded *Lipschitzian* domain in $\mathbb{R}^3$ with piecewise smooth boundary $\partial\Omega$ and ω denotes a mid-surface (i.e., the plane with $z = 0$) in $\mathbb{R}^2$ with piecewise smooth line boundary $\partial\omega$.

We assume that the composition fractions are functions of z only, the essential boundary region $\partial\Omega_D$ is restricted to the top and bottom surfaces $\Gamma_\pm = \{\boldsymbol{x} : (x, y) \in \omega,\ z = \pm d\}$ while the natural boundary region $\partial\Omega_N$ is assigned to the lateral surface $\Gamma_\ell = \partial\omega \times (-d, d)$. Furthermore, we make the following additional assumptions for our study:

- The layers are perfectly bonded.
- The strains are small.
- The Kirchhoff–Love hypothesis holds.
- The body is initially in stress-free state and has uniform room temperature T_0.

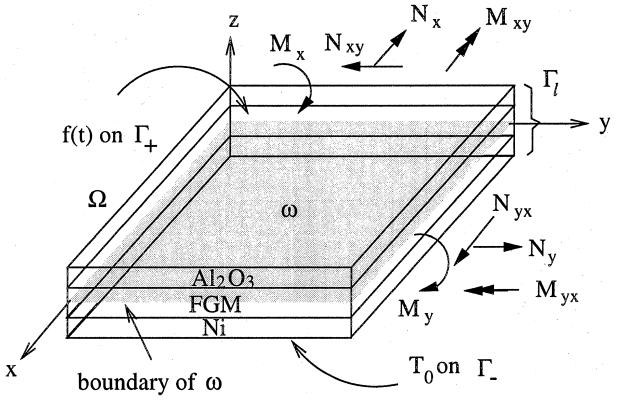

Fig. 6. A three-dimensional symmetric FGM layered composite plate of uniform thickness and in-plane thermal-stress resultants.

3.1. Basic theories

The governing equations for time-dependent temperature field $T(\boldsymbol{x};t)$ are composed of a general heat-diffusion equation based on *Fourier's* law, and the initial and boundary conditions (i.e. initial-boundary value problem):

$$\begin{aligned}
&\rho c\frac{\partial T}{\partial t}-\nabla\cdot(k\nabla T)=\frac{\partial q}{\partial t}\quad \text{in } \Omega,\quad t\in(0,t^*],\\
&T(\boldsymbol{x};t)=T_0\quad \text{at } t=0,\\
&T(x,y,-d;t)=T_0\quad \text{for } t\in(0,t^*],\\
&T(x,y,+d;t)=f(x,y;t)\quad \text{for } t\in(0,t^*],\\
&(-k\nabla T\cdot\boldsymbol{n})|_{(\partial\Omega_N;t)}=\vartheta(\boldsymbol{x};t)\quad \text{for } t\in(0,t^*].
\end{aligned}\tag{9}$$

Here, c and κ indicate the specific heat and the thermal conductivity, respectively, while $q\in L^2(\Omega)$ and t^* denote the internal heat source and the time interval under consideration. Thermal and mechanical quantities are constants in the metal and ceramic layers, but functions of z in the FGM layer. It is obvious all material properties are $\mathscr{C}^0(\bar{\Omega})$ functions. In addition, constant room temperature T_0 is applied to the bottom surface Γ_- while varying temperature $f(x,y;t)\in L^2(\partial\Omega_{\mathrm{D}})$ is applied to the top surface Γ_+, and external heat fluxes $\vartheta\in L^2(\partial\Omega_N)$ are applied to Γ_ℓ.

After obtaining the temperature field $T(\boldsymbol{x};t)$, we compute thermal-stress distributions. In order to calculate them, we must derive the suitable equations. First, according to assumptions made so far, the non-vanishing strain components are expressed by

$$\left\{\begin{array}{c}\varepsilon_x\\ \varepsilon_y\\ \gamma_{xy}\end{array}\right\}_{(\boldsymbol{x};t)}=\left\{\begin{array}{c}\varepsilon_x^0\\ \varepsilon_y^0\\ \gamma_{xy}^0\end{array}\right\}_{(x,y;t)}+z\cdot\left\{\begin{array}{c}\kappa_x^0\\ \kappa_y^0\\ \kappa_{xy}^0\end{array}\right\}_{(x,y;t)},\tag{10}$$

where $\{\varepsilon_x^0,\varepsilon_y^0,\gamma_{xy}^0\}$ are in-plane strains and $\{\kappa_x^0,\kappa_y^0\}$, κ_{xy}^0 are in-plane curvatures and torsion, respectively, of the mid-surface. Using the stress–strain relations of plane-stress problems, we have the non-vanishing stress components given by

$$\left\{\begin{array}{c}\sigma_x\\ \sigma_y\\ \tau_{xy}\end{array}\right\}_{(\boldsymbol{x};t)}=\frac{E}{(1-\nu^2)}\left[\begin{array}{ccc}1&\nu&0\\ \nu&1&0\\ 0&0&(1-\nu)\end{array}\right]_{(z)}\left\{\begin{array}{c}\varepsilon_x^0+z\cdot\kappa_x^0\\ \varepsilon_y^0+z\cdot\kappa_y^0\\ \gamma_{xy}^0+z\cdot\kappa_{xy}^0\end{array}\right\}-\left(\frac{\alpha E}{1-\nu}\right)_{(z)}\left\{\begin{array}{c}\Delta T\\ \Delta T\\ 0\end{array}\right\},\tag{11}$$

where ΔT is $(T(\boldsymbol{x};t)-T_0)$.

In order to compute the thermal stresses due to the temperature gradient, the applied external force $\boldsymbol{F}^{\mathrm{ext}}$ and moment $\boldsymbol{M}^{\mathrm{ext}}$ (thickness-integrated/unit area in ω), we must determine three in-plane strains, two in-plane curvatures and a torsion. First, we denote six across-the-thickness thermal stress resultants, for which a notation convention is shown in Fig. 6, by

$$\left\{\begin{array}{c}N_x\\ N_y\\ N_{xy}\end{array}\right\}=\int_{-d}^{d}\left\{\begin{array}{c}\sigma_x\\ \sigma_y\\ \tau_{xy}\end{array}\right\}\mathrm{d}z,\quad \left\{\begin{array}{c}M_x\\ M_y\\ M_{xy}\end{array}\right\}=\int_{-d}^{d}\left\{\begin{array}{c}\sigma_x\\ \sigma_y\\ \tau_{xy}\end{array}\right\}z\,\mathrm{d}z\tag{12}$$

and we introduce moment-of-inertia-like quantities $\{H_i,\ I_i,\ J_i,\ L_i\}$

$$\begin{aligned}
&H_i(x,y)=\int_{-d}^{d}\frac{\nu E}{(1-\nu^2)}z^i\,\mathrm{d}z,\qquad I_i(x,y)=\int_{-d}^{d}\frac{E}{(1-\nu^2)}z^i\,\mathrm{d}z,\\
&J_i(x,y;t)=\int_{-d}^{d}\frac{\alpha E\Delta T}{(1-\nu)}z^i\,\mathrm{d}z,\qquad L_i(x,y)=\int_{-d}^{d}\frac{E}{(1-\nu)}z^i\,\mathrm{d}z\qquad (i=0,1,2).
\end{aligned}\tag{13}$$

Since the thermal-stress resultants should be statically equivalent to the applied force and moment, it is not difficult to obtain the following system of simultaneous equations for the four unknowns

$$\begin{bmatrix} I_0 & I_1 & H_0 & H_1 \\ I_1 & I_2 & H_1 & H_2 \\ H_0 & H_1 & I_0 & I_1 \\ H_0 & H_2 & I_1 & I_2 \end{bmatrix} \begin{Bmatrix} \varepsilon_x^0 \\ \kappa_x^0 \\ \varepsilon_y^0 \\ \kappa_y^0 \end{Bmatrix} = \begin{bmatrix} F_x^{\text{ext}} + J_0 \\ M_x^{\text{ext}} + J_1 \\ F_y^{\text{ext}} + J_0 \\ M_y^{\text{ext}} + J_1 \end{bmatrix} \tag{14}$$

and the relations for two unknowns given by

$$\begin{aligned} \gamma_{xy}^0 &= \left[-L_2 F_{xy}^{\text{ext}} + L_1 M_{xy}^{\text{ext}} \right] / \mathscr{L}, \\ \kappa_{xy}^0 &= \left[L_1 F_{xy}^{\text{ext}} - L_0 M_{xy}^{\text{ext}} \right] / \mathscr{L}. \end{aligned} \tag{15}$$

Here, $\mathscr{L}$ is defined as $(L_1^2 - L_0 L_2)$.

We then compute thermal-stress field with Eq. (11) at any time and for any application of external forces and moments.

Remark 3.1. *From the relations in Eq.* (15), *we know that* $\{\gamma_{xy}^0, \kappa_{xy}^0\}$ *are time-independent*, *furthermore they are identically zero if no external force and moment are applied.*

Here, we consider a simpler case of $\{\varepsilon_x = \varepsilon_y\}$ and $\{\gamma_{xy} = 0\}$ which corresponds to uniform heating function $f(x, y; t) = f(t)$ and an external forces and moments satisfying $\{F_x^{\text{ext}} = F_y^{\text{ext}} = F^{\text{ext}}\}$, $\{M_x^{\text{ext}} = M_y^{\text{ext}} = M^{\text{ext}}\}$ and $\{F_{xy}^{\text{ext}} = M_{xy}^{\text{ext}} = 0\}$. Then, using the fact of $\{\sigma_x = \sigma_y = \sigma\}$ and $\{\tau_{xy} = 0\}$, we have

$$\sigma(z; t) = \frac{E(z)}{(1 - \nu(z))} \left[\varepsilon^0(z) + z \cdot \kappa^0(z) - \alpha(z) \Delta T(z; t) \right], \tag{16}$$

where two unknowns are

$$\begin{aligned} \varepsilon^0 &= \left[-\tilde{I}_2 (J_0 - F^{\text{ext}}) + \tilde{I}_1 (J_1 + M^{\text{ext}}) \right] / \tilde{\mathscr{I}}, \\ \kappa^0 &= \left[\tilde{I}_1 (J_0 - F^{\text{ext}}) + \tilde{I}_0 (J_1 + M^{\text{ext}}) \right] / \tilde{\mathscr{I}}. \end{aligned} \tag{17}$$

Here, the $\tilde{I}_i$ are defined by substituting $E/(1 - \nu^2)$ in Eq. (13) with $E/(1 - \nu)$ while $\tilde{\mathscr{I}}$ is defined as $(\tilde{I}_1^2 - \tilde{I}_0 \tilde{I}_2)$.

The symmetric matrix in Eq. (13) containing $\{H_i, I_i\}$ should be positive definite for non-trivial solutions. However, Eqs. (15) and (17) do not become singular because the two determinants $\mathscr{L}$ and $\tilde{\mathscr{I}}$ do not vanish for $\nu \neq -1$, as proved in Lemma 3.1.

Lemma 3.1. *For* $\nu \neq -1$, *the two determinants* $\mathscr{L}$ *and* $\tilde{\mathscr{I}}$ *defined above are always negative real numbers* (*i.e.* $\mathscr{L}, \tilde{\mathscr{I}} \in \mathbb{R}^-$).

Proof. Let denote $zE(z)/(1 - \nu)$ and $zE(z)/(1 - \nu^2)$ by $z\tilde{E}(z)$, then

$$z\tilde{E}(z) = \begin{cases} \mathbb{R}^-, & z < 0, \\ 0, & z = 0, \\ \mathbb{R}^+, & z > 0 \end{cases} \tag{18}$$

and which implies

$$\left(\int_{-d}^{d} z\tilde{E}(z) \, \mathrm{d}z \right)^2 < \left(\int_{-d}^{d} |z\tilde{E}(z)| \, \mathrm{d}z \right)^2.$$

Furthermore, from *Cauchy–Schwartz* inequality, we have

$$\left(\int_{-d}^{d} |z\tilde{E}(z)| \, \mathrm{d}z \right)^2 \leqslant \|z\|_{L^2(-d,d)}^2 \|\tilde{E}(z)\|_{L^2(-d,d)}^2. \tag{19}$$

Then, the following inequality holds

$$\left(\int_{-d}^{d} z\tilde{E}(z)\,\mathrm{d}z \right)^2 < \|z\|^2_{L^2(-d,d)} \|\tilde{E}(z)\|^2_{L^2(-d,d)} < \int_{-d}^{d} \tilde{E}(z)\,\mathrm{d}z \int_{-d}^{d} z^2\tilde{E}(z)\,\mathrm{d}z. \tag{20}$$

Finally, we have $\mathscr{L}$, $\tilde{\mathscr{I}} \in \mathbb{R}^-$. □

3.2. Parametric investigation

We now define two quantities for examining the thermal-stress characteristics of FGM member χ in the previously defined hierarchical families. In fact, the relative thickness of heat-resisting layered composites used in most engineering applications is thin, and furthermore major concerns focus on the distributions of axial stress components σ_x and σ_y through the thickness.

By denoting the thermal-stress distribution of axial stress component $\sigma_\alpha(\alpha = x, y)$ of FGM members $\mathscr{M}$ by $\sigma_\alpha(\mathscr{M})$, we define two quantities as the basis for parametric investigation on the effects of the two parameters.

The first quantity, the *local sharpness* $\Delta(\mathscr{M})$ of the thickness-wise distributions of axial thermal-stress components $\sigma_\alpha(\mathscr{M})$, is defined as

$$\Delta(\mathscr{M}) = {}^{\text{def}} \frac{1}{2|z_0 - z^*|}. \tag{21}$$

Referring to Fig. 7, z_0 is a vertical location in the FGM layer at which thermal-stress reaches the steepest value convex or concave, while z^* is defined as its closest neighborhood location with a value of $\sigma^*_\alpha = \sigma^0_\alpha - \Delta\sigma_\alpha$. Here, $\Delta\sigma_\alpha$ is defined as a relative difference between σ^0_α and $\sigma^0_\alpha/\sqrt{2}$. When the steepest side intersects with the bottom or the top side of FGMs, we extrapolate the thermal-stress distribution to calculate z^*. The *thickness-averaged L^2-norm* $\|\sigma_\alpha(\mathscr{M})\|_{L^2(-d_\mathrm{m},d_\mathrm{m})}$, the other quantity, is defined by

$$\|\sigma_\alpha(\mathscr{M})\|_{L^2(-d_\mathrm{m},d_\mathrm{m})} = {}^{\text{def}} \left\{ \frac{1}{2d_\mathrm{m}} \int_{-d_\mathrm{m}}^{d_\mathrm{m}} |\sigma_\alpha(\mathscr{M})|^2\,\mathrm{d}z \right\}^{1/2}, \quad \alpha = x, y. \tag{22}$$

The thermomechanical behavior exhibits the edge effect near the boundary when the dimension of the mid-surface of FGMs is finite. In addition, it varies along the mid-surface under general thermal and mechanical loadings. However, since we are interested in its variations through the thickness with the two defined parameters N and χ, we restrict to the xy-invariant thermomechanical distributions for our parametric analysis. Then, for the functionally graded heat-resisting composites with the composition volume

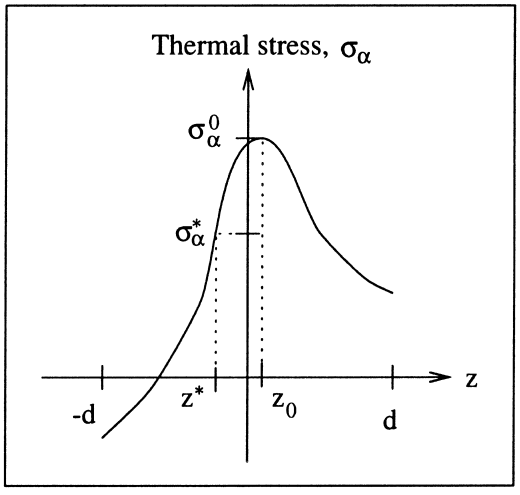

Fig. 7. A definition of local sharpness $\Delta(\mathscr{M})$.

fraction defined in Eq. (1), their thermal-stress distributions satisfy the following properties with respect to the two defined quantities.

Property 3.1. *For a given N, the χ-hierarchical family $\mathscr{F}_H^\chi$ has the following properties (except for relatively small or large N):*

$$\Delta(\mathscr{M}_N^\chi) \text{ decreases as } \chi \to 1,$$
$$\|\sigma_\alpha(\mathscr{M}_N^\chi)\|_{L^2(-d_m,d_m)} \text{ increases as } \chi \to 0, \quad \alpha = x, y.$$

Property 3.2. *The N-hierarchical family $\mathscr{F}_H^N$ exhibits the following property:*

$$\Delta(\mathscr{M}_\chi^N) \to \text{ increases as } N \to 0 \quad \text{or } \infty.$$

4. Formulation of the approximations

An approximation of $T(\boldsymbol{x};t)$ in Eq. (9) involves discretizations both in time and space domains. In this paper, we employ a finite difference method in time and a finite element approximation in space.

4.1. Time discretization and variational formulation

Let us make finite N uniform partitions (or subinterval-wise uniform partitions) in time domain $(0, t^*]$, then we have uniform (or subinterval-wise uniform) time intervals $\Delta t = t^*/N$ and $(N+1)$ time stages $t_n = n\Delta t$, $(n = 0, 1, \ldots, N)$.

For a time discretization, we use the *Crank–Nicolson* method, a first-order time approximation with relatively higher local truncation error $\mathscr{O}(\Delta t)^3$, in which $T_{n+1/2}$ and $(\partial T/\partial t)_{n+1/2}$ at the mid of two time stages t_n and t_{n+1} are

$$\begin{aligned} T_{n+1/2} &= \frac{1}{2}(T_{n+1} + T_n), \\ \left(\frac{\partial T}{\partial t}\right)_{n+1/2} &= \frac{1}{\Delta t}(T_{n+1} - T_n). \end{aligned} \tag{23}$$

Substituting Eq. (23), $(\partial q/\partial t)_{n+1/2}$, $f_{n+1/2}$ and $\vartheta_{n+1/2}$ into the initial-boundary-value problem (9), we have a sequence of semi-discrete converted boundary value problems for N time stages t_n $(n = 0, 1, 2, \ldots, N-1)$:

$$\begin{aligned} &\frac{\rho c}{\Delta t}(T_{n+1} - T_n) - \nabla \cdot \left\{ k \nabla \left(\frac{T_{n+1} + T_n}{2} \right) \right\} = \left(\frac{\partial q}{\partial t} \right)_{n+1/2} \quad \text{in } \Omega, \\ &T_{n+1/2}(\boldsymbol{x}) = T_0 \quad \text{on } y = -d, \\ &T_{n+1/2}(\boldsymbol{x}) = f_{n+1/2}(x, y) \quad \text{on } y = +d, \\ &(-k \nabla T \cdot \boldsymbol{n})_{n+1/2}(\boldsymbol{x}) = \vartheta_{n+1/2}(\boldsymbol{x}) \quad \text{on } \partial\Omega_N. \end{aligned} \tag{24}$$

It is well known that the *Crank–Nicolson* scheme, while unconditionally convergent, produces oscillatory results unless the time step is appropriately selected.

The converted boundary value problem (24) characterizes successively the temperature distribution $T(\boldsymbol{x}; t_{n+1})$ at time t_{n+1} with the previously obtained solution $T(\boldsymbol{x}; t_n)$ at time t_n and the known boundary data of T_0, $f_{n+1/2}$ and $\vartheta_{n+1/2}$.

Now, we establish a weighted residual variational formulation for the solution $T(\boldsymbol{x}; t_{n+1})$ at the $(n+1)$th time stage. First, we define the space $V(\Omega)$ of admissible test temperature fields such that every function v in $V(\Omega)$ has finite thermal strains and its trace on $\partial\Omega_D$ vanishes

$$V(\Omega) = \left\{ v(\boldsymbol{x}) : v(\boldsymbol{x}) \in H^1(\Omega) | \gamma_D v = 0 \right\} \tag{25}$$

with γ_{D} defined as a trace operator, $\gamma_{\mathrm{D}} : H^1(\Omega) \to H^{1/2}(\partial\Omega_{\mathrm{D}})$. On the other hand, the trial function space $\tilde{V}_{n+1}(\Omega)$ for the $(n+1)$th time stage is defined as a linear manifold of $V(\Omega)$

$$\tilde{V}_{n+1}(\Omega) = V(\Omega) + \{w^*\}_{n+1}, \tag{26}$$

where $\{w^*\}$ are extended $H^1(\Omega)$ functions satisfying $w^*|_{\Gamma_-} = T_0$ and $w^*|_{\Gamma_+} = f_{n+1/2}$. We note that the trial function space is time-stage-dependent owing to different trace data on Γ_+ at different time stages, while the test function space is time-stage-dependent.

As usual, multiplying the converted partial differential equation by a test function Q and integrating over the domain Ω, we arrive at a sequence of N abstract boundary value problems:

$$\begin{aligned} &\text{Given } T_0 \in \tilde{V}_0(\Omega), \text{ find } T_{n+1} \in V(\Omega) + \{w^*\}_{n+1} \text{ such that} \\ &a(T_{n+1}, Q) = \ell(Q) \quad \forall Q \in V(\Omega) \quad (n = 0, 1, 2, \ldots, N-1). \end{aligned} \tag{27}$$

Here, a bilinear functional $a(\cdot,\cdot) : V(\Omega) \times V(\Omega) \to \mathbb{R}$ and a linear functional $\ell(\cdot) : V(\Omega) \to \mathbb{R}$ are, respectively, defined by $(\mathrm{d}x = \mathrm{d}x\,\mathrm{d}y\,\mathrm{d}z)$.

$$\begin{aligned} a(T_{n+1}, Q) &= \int_\Omega \rho c T_{n+1} Q \,\mathrm{d}x + \frac{\Delta t}{2} \int_\Omega k(\nabla T_{n+1} \cdot \nabla Q)\,\mathrm{d}x, \\ \ell(Q) &= \int_\Omega \rho c T_n Q \,\mathrm{d}x - \frac{\Delta t}{2} \int_\Omega k(\nabla T_n \cdot \nabla Q)\,\mathrm{d}x + \int_\Omega \dot{q}_{n+1/2} Q \,\mathrm{d}x - \Delta t \int_{\partial\Omega_N} \vartheta_{n+1/2} Q \,\mathrm{d}x. \end{aligned} \tag{28}$$

It is well known, from the *Lax–Milgram* theorem, that problem (27) is well posed and the solution depends continuously on data.

4.2. Finite element approximations

Since finite element approximations of problem (27) are standard, we do not describe the details on the procedure. Along the standard procedure, one arrives at the full-discrete finite element approximation, the well-known *Crank–Nicolson–Galerkin* scheme. For the detailed analysis on the stability and consistency of this scheme, see [15,19].

As is well known, this scheme produces oscillatory results when the time step is not small enough, particularly for the problem showing sudden changes in its time response by impulsive heating loads or abrupt changes in the boundary condition. This is because one tries to reach directly at the steady state with a larger time step, and such a phenomenon prevails as the largest eigenmode (i.e., one of the shortest wavelength) dominates, such as exponential decay/or increase in the transient response. One of these situations in the heat diffusion problem is the problem subjected to thermal shock.

In order to determine the critical time step for our study, we examine finite-element eigenvalues in the free response of problem (9). The free response is expressed by

$$T(\boldsymbol{x}; t) = X(\boldsymbol{x}) \cdot \mathrm{e}^{-\lambda t} \tag{29}$$

with eigenvalues λ_{mn} (assuming constant ρ, c and κ) given by

$$\lambda_{mn} = \left[\left(\frac{m\pi}{L_x} \right)^2 + \left(\frac{n\pi}{L_y} \right)^2 \right] \frac{\kappa}{\rho c}, \quad m, n = 1, 2, \ldots, \tag{30}$$

where, L_x and L_y denote the characteristic lengths of $\Omega \in \mathbb{R}^N$ (when N is 2). Then, for a uniform finite element mesh with varying material constants, the largest eigenvalue is

$$\lambda_{\max} \approx N \left[\frac{\pi}{d} \right]^2 \left(\frac{\kappa}{\rho c} \right)_{\max}, \tag{31}$$

where d denotes a distance between two adjacent nodes. On the other hand, for a non-uniform mesh with varying material constants, it is

$$\lambda_{\max} \approx N\left[\frac{\pi}{d_{\min}}\right]^2 \left(\frac{\kappa}{\rho c}\right)_{\max}. \tag{32}$$

In order to prevent oscillations in such a largest eigenmode, it has been suggested that one use the time step satisfying

$$\Delta t_{\text{crit}} \cdot \lambda_{\max} \approx 2 \cdot C_{\text{f}} \tag{33}$$

with a correction parameter C_{f} of $2 \sim 3$ [4]. The critical time step depends on the material properties and the size of finite elements. In particular, it has a proportional relation to the square of minimum size of finite elements.

For the entire time interval, use of the uniform time-stepping method with the time step corresponding to the critical eigenmode may lead to a very expensive numerical computation. In fact, the time-response is characterized by dominant several eigenmodes, and the range of eigenmodes dominating the time-response varies along the time duration in most cases. Therefore, it would be advisable to adopt the graded time-stepping method (similar to an irregular mesh construction in spatial approximations) or to divide the entire time interval into several subintervals with different uniform time steps.

5. Numerical experiments

To investigate the thermo-elastic characteristics of FGMs, we simulate a symmetric two-dimensional functionally graded composite beam of uniform thickness $2d = 10$ mm, $2L = 1$ mm, and unit depth. As for the metal and ceramic layers, we select Ni and Al_2O_3, respectively, and their thermal and mechanical properties are summarized in Table 1.

Referring to Fig. 2, a room temperature T_0 of 290 K is kept at the bottom surface while a heating temperature $f(t)$ shown in Fig. 8(a) is applied on the top surface. Furthermore, the condition of no temperature gradient is assigned at the left- and right-hand sides in order to exclude the boundary effect (i.e., for the x-invariant temperature field). With this FGM model, we analyze the transient and the steady-state response in temperature and thermal-stress fields. As for the values of the two parameters, χ and N, we take N of 0.3, 0.7, 1, 5, 10 and 100 for each χ of 0.2, 0.5, 0.7 and 1.

For finite element approximations, we make six uniform partitions in the horizontal direction and three layer-wise uniform partitions (i.e. 3×20 partitions) in the thickness direction so that a total of 360 (6×60) almost uniform biquadratic tensor-product-type elements are assigned regardless of the combination of the two defined parameters.

For a given heating condition, numerical and geometry data, we examine the time step according to the previous discussion. For the x-invariant temperature distribution through the thickness and the layer-wise uniform mesh using biquadratic elements, we obtain $\Delta t_{\text{crit}} \approx 0.0001$ s for the largest eigenmode from Eqs. (31) and (33) (with C_{f} of 3). On the other hand, for the smallest eigenmode, we obtain $\Delta t \approx 1$ s (with C_{f} of 1). However, since the suitable time-step depends definitely on the dominant eigenmode in the temperature response, we first examine the temperature-time histories of the problem under consideration with different

Table 1
Numerical data of thermal and mechanical properties of Ni and Al_2O_3

Properties	Constituents	
	Ni	Al_2O_3
Density (kg/m^3)	8900.0	3970.0
Young's modulus (GPa)	199.5	393.0
Poisson's ratio	0.3	0.25
Specific heat (J/kg K)	444.0	775.0
Thermal conductivity (W/m K)	90.7	30.1
Thermal expansion coefficient (°C $\times 10^{-6}$)	13.3	8.8

uniform time steps Δt of 0.1, 1 and 5 s. For this preliminary test, we use χ of 0.2 and N of 0.3 because this combination is expected to show the representative behavior to determine the time step for our numerical experiments.

We compute and plot the temperature-time histories at the upper interface of the graded-layer (i.e. at the point p in Fig. 8, which are depicted in Fig. 9. From the numerical information together with the Δt_{crit}, we see that the system response is not dominated by the largest eigenmode, and furthermore it is characterized by different eigenmodes for different subintervals. We thus divide the entire time interval into three subintervals I(0–5 s), II(5–10 s) and III(10–20 s), as shown in Fig. 8. For the three subintervals, we use different uniform time steps of 0.05, 0.1 and 1 s, respectively.

For the N-hierarchical families with χ of 0.5 and 1.0, we plot the computed temperature distributions at time t_A and t_B in Figs. 10 and 11, where we include the classical layered composite (denoted by CLC in the figures) with a kink at the interface in its temperature distribution. By comparing the transient (at time t_A) and the steady-state (at time t_B) temperature fields, we observe the unsaturated and slightly curved distributions in the Al_2O_3-dominated region at time t_A owing to the relatively smaller thermal conductivity of Al_2O_3. This tendency at time t_A prevails as the relative thickness ratio increases.

When we compare the distributions in Fig. 10 with respect to the parameter N, we observe that the temperature gradient at the FGM–Al_2O_3 interface becomes steeper as N tends to 0. But, as N approaches 100, such a steep gradient prevails at the other interface as N approaches 100. This follows from the previous parametric investigation. In other words, an FGM becomes m-CLC or c-CLC, respectively, as

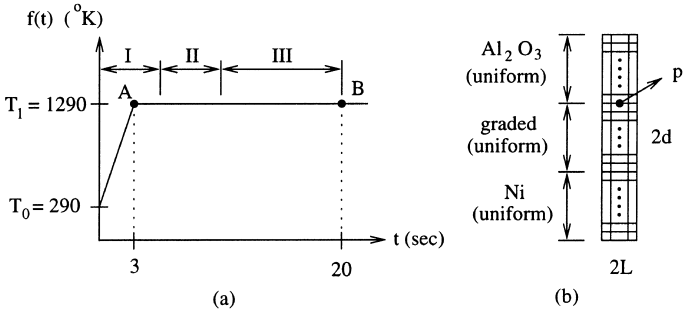

Fig. 8. A heating function $f(t)$ and a FE mesh pattern.

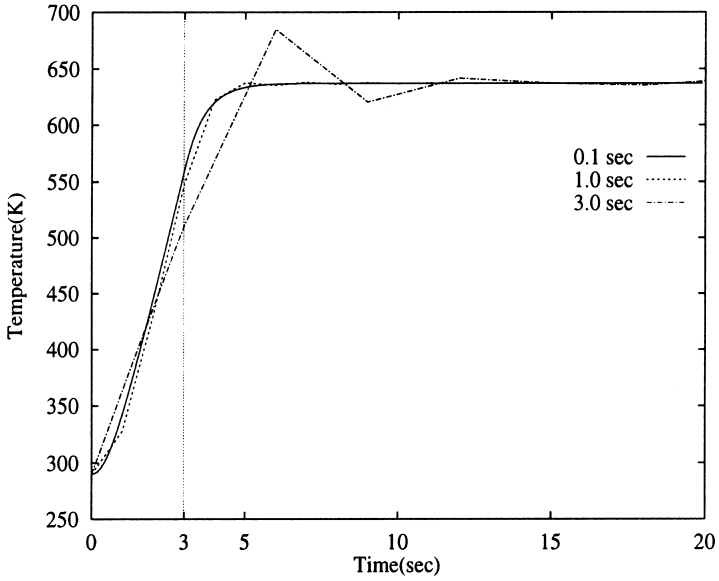

Fig. 9. Temperature–time histories at the point p for three different uniform time steps (χ of 0.2 and N of 0.3).

$N \to 0$ or N approaches ∞. However, as shown in Fig. 11 for the f-FGM, the temperature distributions are smoother and such kinks are not observed, due to the disappearance of the interface with sharp material variation.

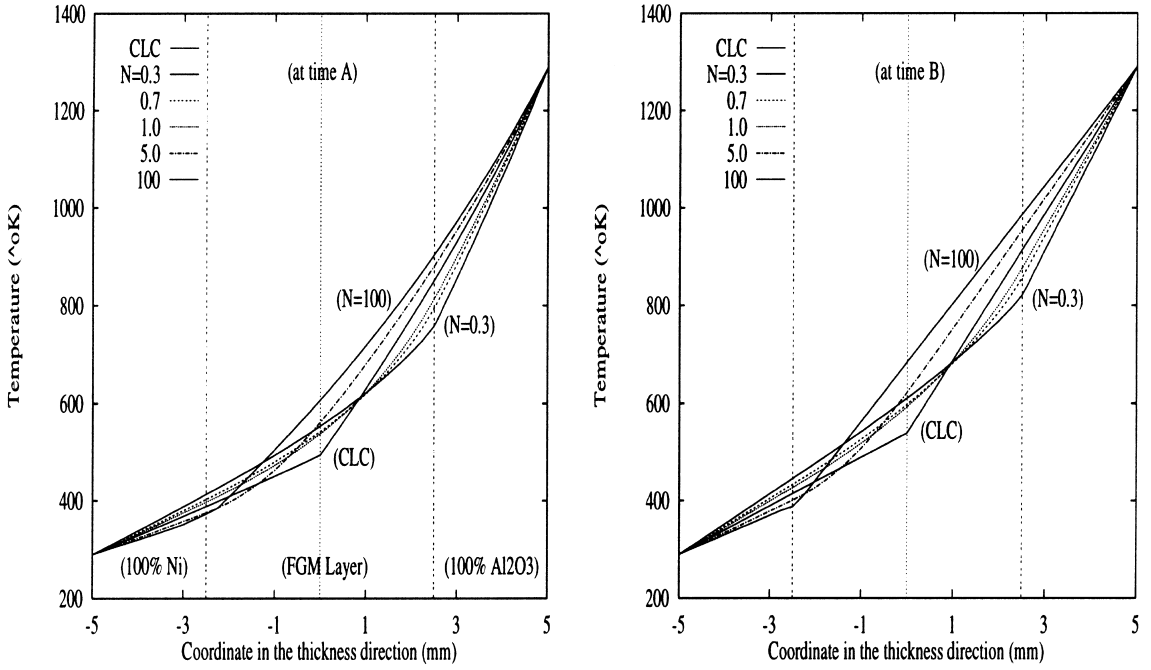

Fig. 10. Temperature distributions of the N-hierarchical members $\mathscr{M}^N_{0.5}$.

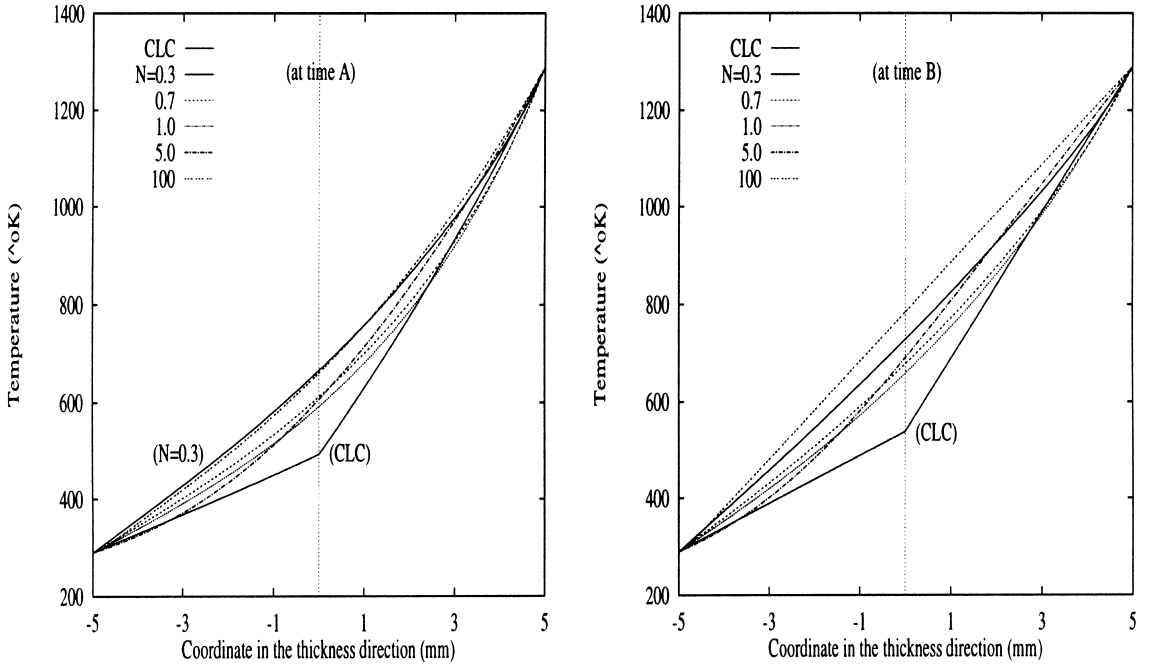

Fig. 11. Temperature distributions of the N-hierarchical members $\mathscr{M}^N_{1.0}$.

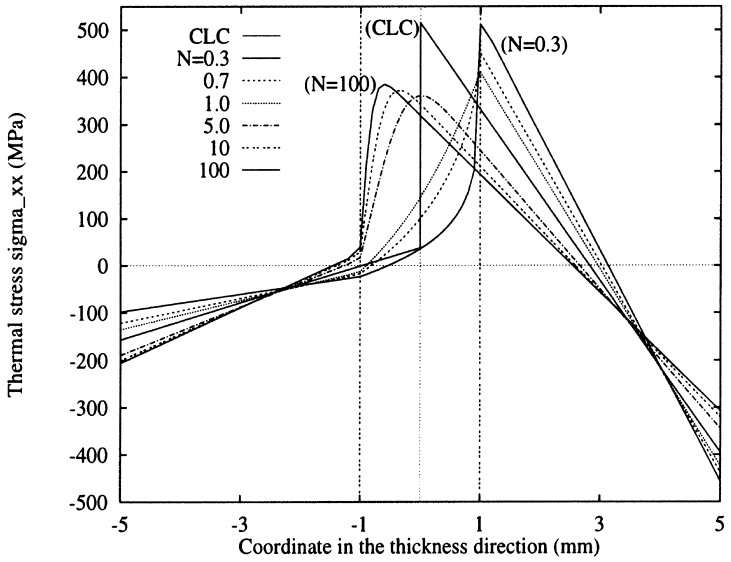

Fig. 12. Thermal-stress (σ_x) distributions of the N-hierarchical members $\mathscr{M}^N_{0.2}$ at time t_B.

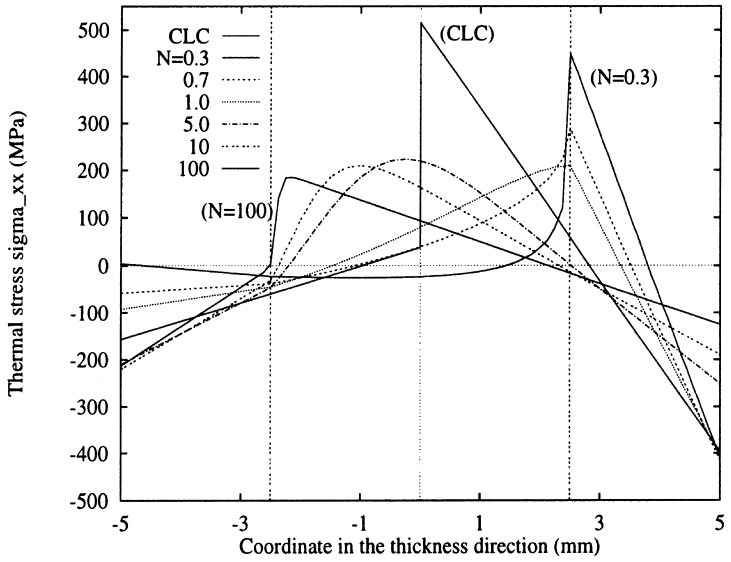

Fig. 13. Thermal-stress (σ_x) distributions of the N-hierarchical members $\mathscr{M}^N_{0.5}$ at time t_B.

For the N-hierarchical families with χ of 0.2, 0.5, 0.7 and 1.0, the computed thermal-stress distributions at time t_A are presented in Figs. 14–16, while those at time t_B are given in Figs. 12, 13, 15 and 17, where the bimaterial composite case is included in order for a comparison purpose. The transient response in thermal-stress, when compared to the steady-state response, shows the slightly curved pattern in the Al_2O_3-dominated region according to the unsaturated curved-distribution of the temperature field. This tendency prevails as N increases. Because the difference in thermal-stress distributions at time t_A and t_B become more considerable as χ increases, due to the extension of Al_2O_3 to the entire composite region, we exclude the trasient distributions for the cases with χ of 0.2 and 0.5.

By examining Fig. 12 of the N-hierarchical family with χ of 0.2, we see thermal-stress concentrations at the FGM–Al_2O_3 interface for relatively small N and at the FGM–Ni interface for relatively large N, respectively. The concentration at the right interface is relaxed as N increases, while the other concentration

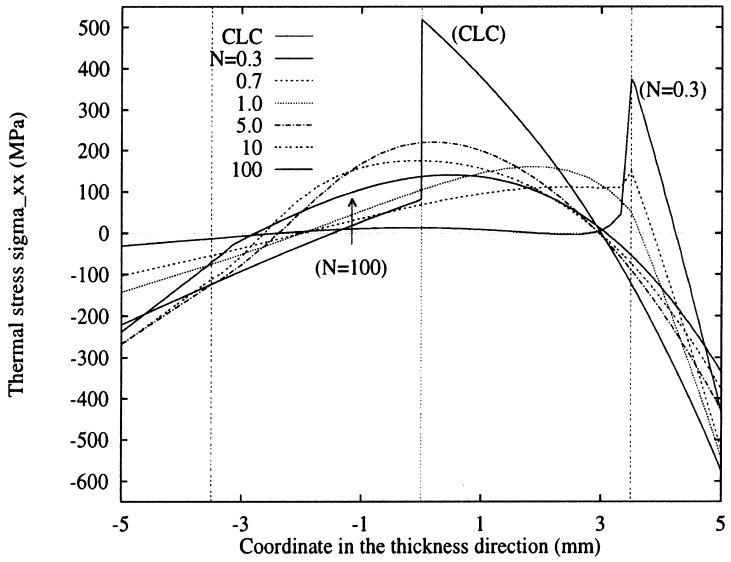

Fig. 14. Thermal-stress (σ_x) distributions of the N-hierarchical members $\mathscr{M}_{0.7}^{N}$ at time t_A.

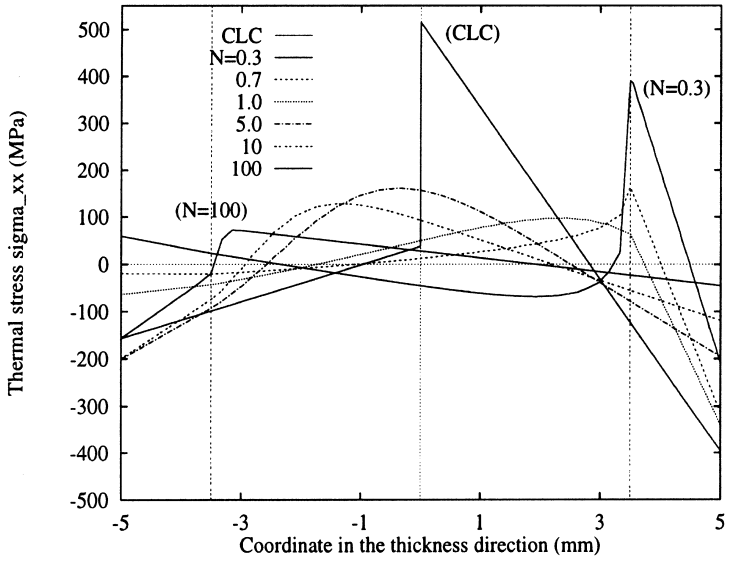

Fig. 15. Thermal-stress (σ_x) distributions of the N-hierarchical members $\mathscr{M}_{0.7}^{N}$ at time t_B.

near the left interface looses as N decreases. This figure represents well the effect of the volume fraction on the thermal-stress behavior near the interface with steep material property variations.

Through the next Figs. 13–17, we observe the effect of the relative thickness ratio on thermal-stress of the N-hierarchical families. Because the difference in thermal-stress distributions at time t_A and t_B is considerable when the relative thickness ratio is large, we include the transient results for χ of 0.7 and 1.0. When we compare the transient and steady-state thermal-stress behavior, the difference becomes considerable near the FGM–Ni interface (near the bottom surface for the f-FGM) as N increases. On the other hand, when we examine the thermal-stress distributions with respect to the relative thickness ratio (i.e., for the χ-hierarchical families), we first see that the stress concentration near the FGM–Ni interface becomes monotonically relaxed as χ increases. We note here that the f-FGM with N of 100 displays a convex concentration in Fig. 16 and a sudden drop from the almost zero stress level in Fig. 17, respectively, near the bottom surface. The stress concentration at FGM–Ni interface for the relatively large N seems to be

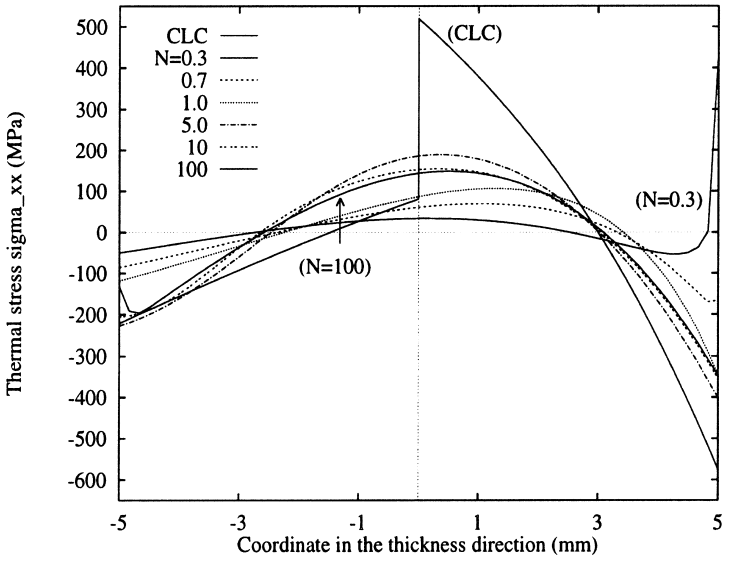

Fig. 16. Thermal-stress (σ_x) distributions of the N-hierarchical members $\mathscr{M}^N_{1.0}$ at time t_A.

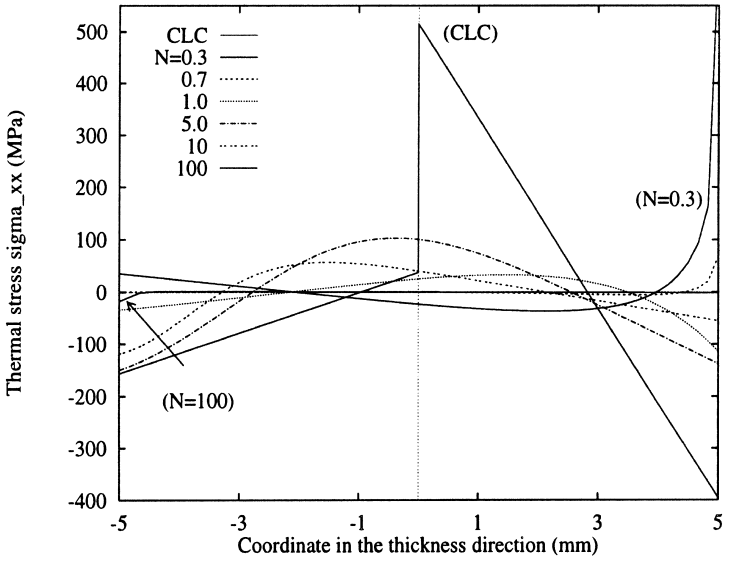

Fig. 17. Thermal-stress (σ_x) distributions of the N-hierarchical members $\mathscr{M}^N_{1.0}$ at time t_B.

relaxed, but not for considerably small $N \leqslant 0.7$. For the χ-hierarchical members $\mathscr{M}^\chi_{0.3}$ and $\mathscr{M}^\chi_{0.7}$, the stress concentrations remain unrelaxed even when χ is 1.0.

Fig. 18 shows the variations of the estimated thickness-averaged L^2-norm of thermal-stress distributions in the middle FGM layer at time t_A and t_B, respectively. As the relative thickness ratio $1/\chi$ increases, the values estimated at both time points increases monotonically for every χ-hierarchical member, which implies that the resulting thermal-stress tends to concentrate in the middle FGM layer as the FGM layer becomes thinner. This is consistent with Property 3.1 in Section 3.2.

The last figures Figs. 19 and 20 show the numerical results concerned with the local sharpness $\Delta(\mathscr{M})$ for the χ- and N-hierarchical families at time t_A and t_B, respectively. The estimated local sharpnesses of the N-hierarchical families are presented in Fig. 19, where the estimated values, except for $\mathscr{M}^\chi_{0.3}$, $\mathscr{M}^\chi_{0.7}$ and $\mathscr{M}^\chi_{100}$, decrease uniformly as χ increases. For those FGM members, it is not relaxed but rather increases

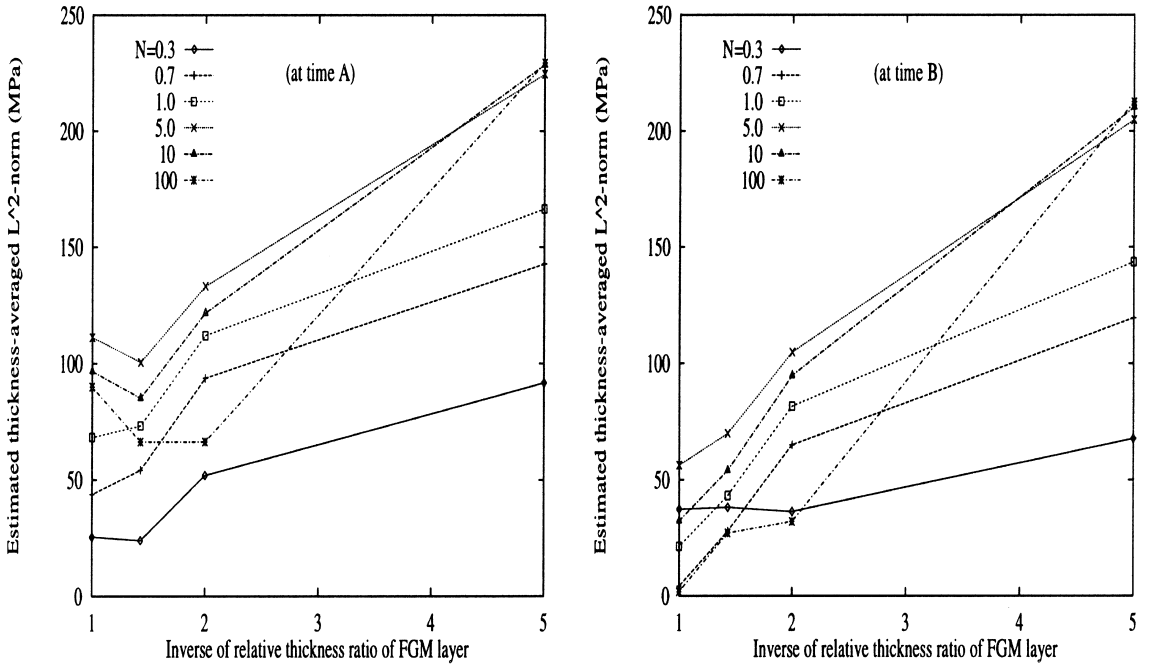

Fig. 18. A variation of $\|\sigma_x(\mathscr{M}_N^\chi)\|_{L^2(-d_m,d_m)}$ along to the relative thickness ratio χ.

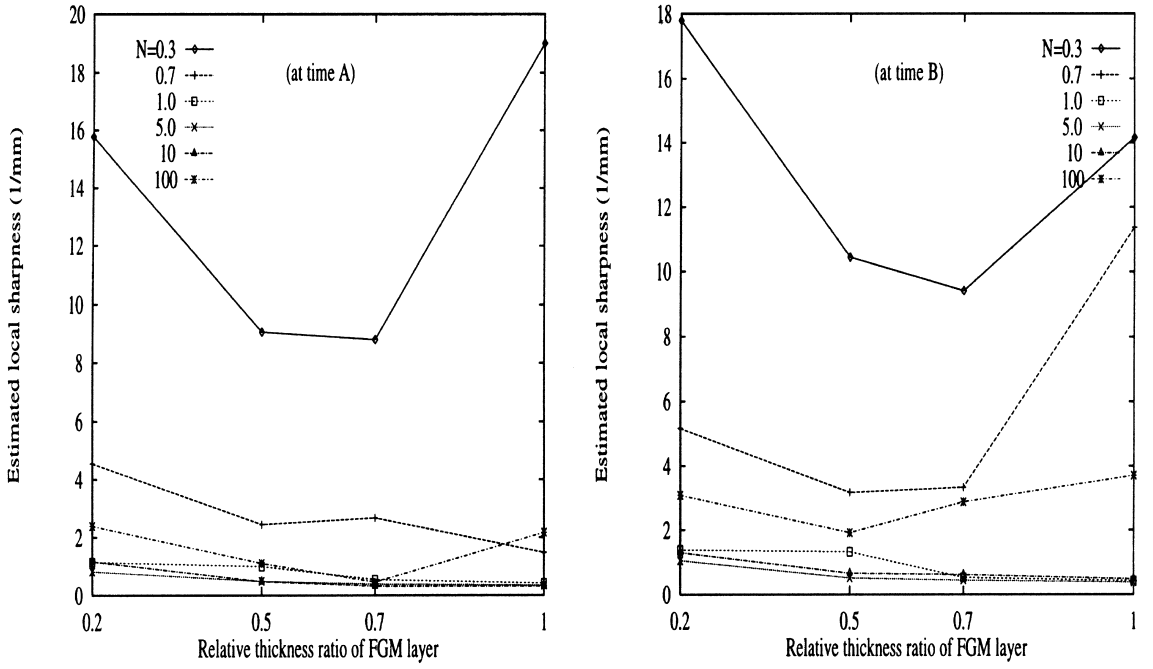

Fig. 19. A variation of $\Delta(\mathscr{M}_N^\chi)$ along to the relative thickness ratio χ.

significantly (except for the $\mathscr{M}_{0.7}^\chi$ at time t_A). This is because the stress concentrations at the FGM–Al_2O_3 interface (for $N \leqslant 0.7$) and the FGM–Ni interface (for $N \geqslant 100$) do not disappear as χ increases, and which illustrates the previously described Property 3.1. The estimated results for the N-hierarchical families are shown in Fig. 20 (where, *RTR* refers to *Relative Thickness Ratio* χ). As declared in Property 3.2, the local

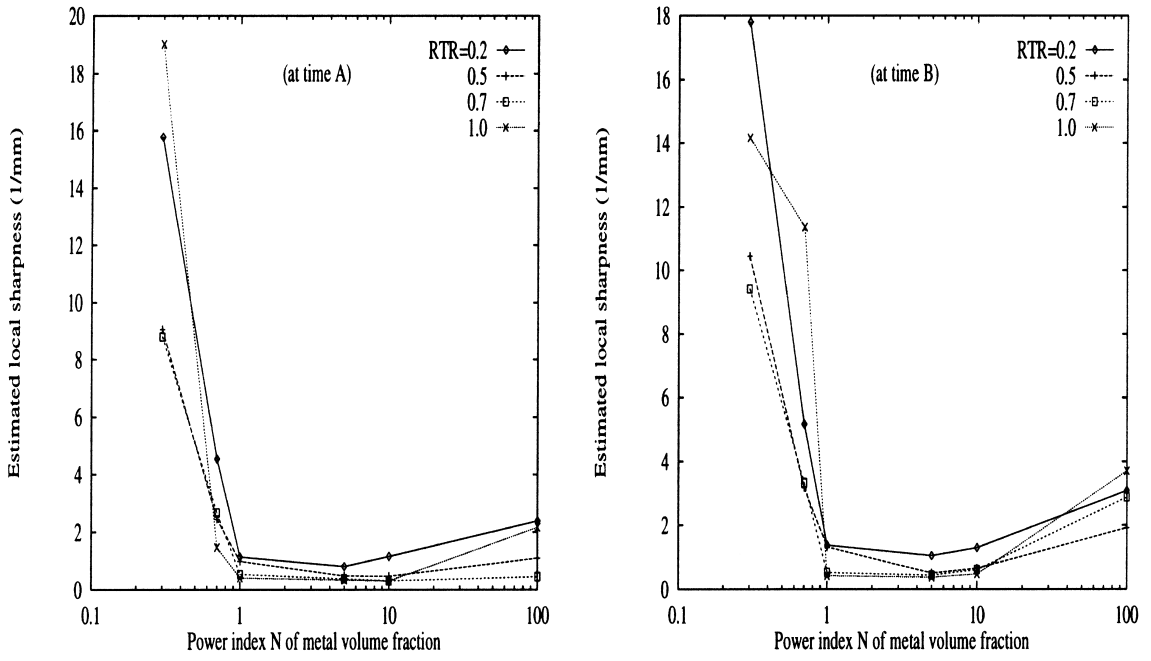

Fig. 20. A variation of $\Delta(\mathscr{M}_{\chi}^{N})$ along to the metal volume fraction parameter N.

sharpness of the N-hierarchical family increases as $N \to 0$ or $N \to \infty$. However, the rate of its increase for $N \to \infty$ is much lower than for $N \to 0$, and this slowness becomes more critical at the transient stage.

6. Conclusions

From the numerical results, we observe that thermomechanical characteristics, such as temperature and thermal-stress distribution, the local sharpness and the thickness-averaged L^2-norm, are quite different for various combinations of the two parameters, N and χ. However, the temperature and thermal-stress distributions vary in a sequential manner with respect to the two parameters, and the estimated quantities $\|\sigma_x(\mathscr{M})\|_{L^2(-d_m,d_m)}$ and $\Delta(\mathscr{M})$ of thermal stresses follow from Properties 3.1 and 3.2. Furthermore, the difference in thermal characteristics between the transient and the steady-state stages is noticeable, especially for large χ and N.

Except for the relatively small or large N, the temperature and thermal-stress distributions become smoother as the relative thickness approaches unity. In the N-hierarchical families, the stress concentration prevails at the FGM–Al_2O_3 interface as N tends to zero while near the FGM–Ni interface as N goes up. Compared to the classical layered composite, FGMs except for the three limiting cases ($N \to 0$, $+\infty$ and $\chi \to 0$) exhibit considerable improvement in the temperature and thermal-stress distributions. This is due primarily to the enforcement of continuity in material properties through the thickness.

Based on our theoretical and numerical results, the selection of optimal (at least, quasi-optimal) combinations of the two parameters satisfying the predefined specification for heat-resisting FGM composites under given thermal circumstances would be worthwhile, and which represents a topic that deserves future work.

Acknowledgements

The financial support given to the first author (JRC) by Pusan National University in Korea under the *Grant-in-Scientific-Assistance* (May 1997–April 2001) is gratefully acknowledged. The second author,

J.T. Oden, acknowledges the support of his work by ONR, under Grant N00014-99-1-0124. The authors would like to thank the anonymous referees for their valuable comments.

Appendix A

According to the modified rule of mixtures, the Young's modulus of graded two-phase composites is given by

$$E = \left[V_{\mathrm{m}}E_{\mathrm{m}}\left(\frac{q+E_{\mathrm{c}}}{q+E_{\mathrm{m}}}\right) + (1-V_{\mathrm{m}})E_{\mathrm{c}}\right] \Big/ \left[V_{\mathrm{m}}\left(\frac{q+E_{\mathrm{c}}}{q+E_{\mathrm{m}}}\right) + (1-V_{\mathrm{m}})\right]. \tag{A.1}$$

By denoting two phases in Fig. 5 by m and p together with the parameter $c = h/a$, we have the volume fraction of the second phase p

$$c = V_{\mathrm{p}}^{-1/3} - 1. \tag{A.2}$$

Then, according to the unit cell approximation, we calculate the Young's modulus of two-phase composites using

$$E = \frac{(E_{\mathrm{p}}E_{\mathrm{m}} - E_{\mathrm{m}}^2)(1 - V_{\mathrm{p}}^{1/3} + V_{\mathrm{p}}) + E_{\mathrm{m}}^2}{E_{\mathrm{p}} + (E_{\mathrm{m}} - E_{\mathrm{p}})V_{\mathrm{p}}^{1/3}} \tag{A.3}$$

and the Poisson's ratio by

$$v = \frac{1}{(1+c)^2}\left[\frac{(v_{\mathrm{p}}E_{\mathrm{m}} + cv_{\mathrm{m}}E_{\mathrm{p}})}{(E_{\mathrm{m}} + cE_{\mathrm{p}})} + v_{\mathrm{m}}(1+c)^2 - v_{\mathrm{m}}\right]. \tag{A.4}$$

According to the Wakashima–Tsukamoto expressions for the macroscopically isotropic particulate composites, the overall bulk modulus $\bar{K}$ and shear modulus $\bar{\mu}$ are obtained by

$$\bar{K} = K_{\mathrm{m}} + \frac{aV_{\mathrm{c}}K_{\mathrm{m}}(K_{\mathrm{c}} - K_{\mathrm{m}})}{V_{\mathrm{m}}K_{\mathrm{c}} + aV_{\mathrm{c}}K_{\mathrm{m}}}, \tag{A.5}$$

$$\bar{\mu} = \mu_{\mathrm{m}} + \frac{bV_{\mathrm{c}}\mu_{\mathrm{m}}(\mu_{\mathrm{c}} - \mu_{\mathrm{m}})}{V_{\mathrm{m}}\mu_{\mathrm{c}} + bV_{\mathrm{c}}\mu_{\mathrm{m}}}, \tag{A.6}$$

where a and b are

$$a = \frac{K_{\mathrm{c}}(3K_{\mathrm{m}} + 4\mu_{\mathrm{m}})}{K_{\mathrm{m}}(3K_{\mathrm{c}} + 4\mu_{\mathrm{c}})}, \tag{A.7}$$

$$b = \frac{(1+e)\mu_{\mathrm{c}}}{(\mu_{\mathrm{m}} + e\mu_{\mathrm{c}})}, \quad e = (9K_{\mathrm{m}} + 8\mu_{\mathrm{m}})/(6K_{\mathrm{m}} + 12\mu_{\mathrm{m}}). \tag{A.8}$$

The overall mechanical properties are immediately obtained from basic parametric relations

$$\bar{E} = 9\bar{K}\bar{\mu}/(3\bar{K} + \bar{\mu}), \tag{A.9}$$

$$\bar{v} = (3\bar{K} - 2\bar{\mu})/2(3\bar{K} + \bar{\mu}). \tag{A.10}$$

And the overall coefficient of thermal expansion $\bar{\alpha}$ is related to the bulk moduli through *Levin's* relation:

$$\bar{\alpha} = \alpha_{\mathrm{m}} + \frac{(1/\bar{K} - 1/K_{\mathrm{m}})(\alpha_{\mathrm{c}} - \alpha_{\mathrm{m}})}{(1/K_{\mathrm{m}} - 1/K_{\mathrm{c}})}. \tag{A.11}$$

Furthermore, the overall specific heat $\bar{c}$ (neglecting the higher order term) and thermal conductivity $\bar{k}$ are expressed, respectively, by

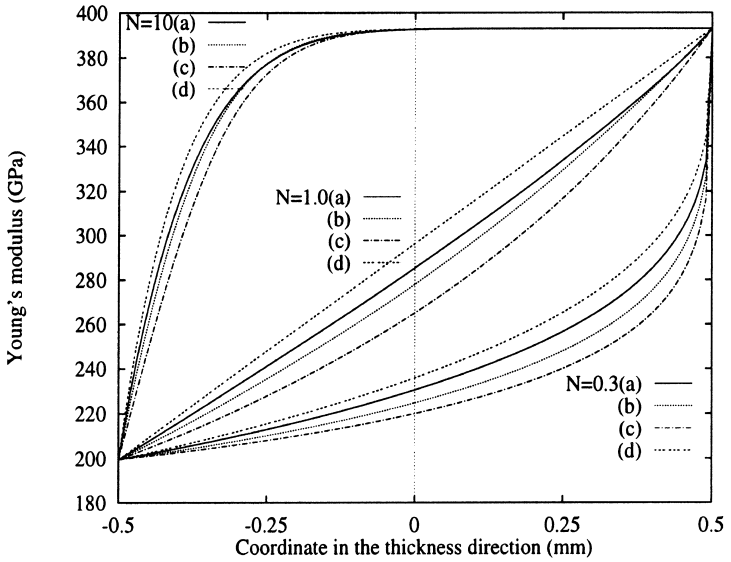

Fig. 21. Distributions of the Young's modulus calculated by the unit cell approach (a), the Wakashima–Tsukamoto expression (b), the modified rule of mixtures (c) and the linear rule of mixtures (d).

$$\bar{c} = c_m + (c_c - c_m)V_c, \tag{A.12}$$

$$\bar{k} = k_m + \frac{k_m V_c (k_c - k_m)}{k_m + (k_m - k_c)V_m/3}. \tag{A.13}$$

A comparison between the distributions of the Young's modulus calculated by the four different approaches is shown in Fig. 21, for which we used the material data given in Table 1. For each volume fraction N, the modified rule produces smaller values than those by the other approaches, while the linear rule of mixtures predicts the stiffest values.

References

[1] A. Bedford, M. Stern, A multi-continuum theory for composite elastic materials, Acta Mech. 14 (1972) 85–102.
[2] R.M. Bowen, D.J. Garcia, On the thermodynamics of mixtures with several temperatures, Int. J. Engrg. Sci. 8 (1970) 63–83.
[3] B. Budiansky, On the elastic moduli of some heterogeneous materials, J. Mech. Phys. Solids 13 (1965) 223–227.
[4] D.S. Burnett, Finite Element Analysis: From Concept to Applications, Addison-Wesley, Reading, MA, 1988.
[5] J.R. Cho, J.T. Oden, A priori modeling error estimates of hierarchical models for elasticity problems for plate- and shell-like structures, Math. Comput. Modelling 23 (10) (1996) 117–133.
[6] T. Chen, G.J. Dvorak, Y. Benveniste, Mori–Tanaka estimates of the overall elastic moduli of certain composites, J. Appl. Mech. 59 (1992) 539–546.
[7] R.M. Christensen, Mechanics of Composite Materials, Wiley/Interscience, New York, 1979.
[8] A.E. Giannakopulos, S. Suresh, M. Olsson, Elastoplastic analysis of thermal cycling: layered materials with compositional gradients, Acta Metall. Mater. 43 (4) (1995) 1335–1354.
[9] M. Grujicic, Y. Zhang, Determination of effective elastic properties of functionally graded materials using voronoi cell finite element method, Mater. Sci. Engrg. A 251 (1998) 64–76.
[10] M. Finot, S. Suresh, C. Bull, S. Sampath, Curvature changes during thermal cycling of a compositionally graded Ni–Al_2O_3 multilayered materials, Mater. Sci. Engrg. A 205 (1996) 59–71.
[11] S. Ghosh, S.N. Mukhopadhyay, A material based finite element analysis of heterogeneous media involving dirichlet tessellations, Comput. Meth. Appl. Mech. Engrg. 104 (1993) 221–247.
[12] Z. Hashin, S. Shtrikman, A variational approach to the theory of the elastic behavior of multiphase systems, J. Mech. Phys. Solids 11 (1963) 127–140.
[13] R. Hill, Elastic properties of reinforced solids: some theoretical principles, J. Mech. Phys. Solids 11 (1963) 357–372.
[14] R. Hill, Self-consistent mechanics of composite materials, J. Mech. Phys. Solids 13 (1965) 213–222.
[15] C. Johnson, Numerical Solution of Partial Differential Equations by the Finite Element Method, Cambridge University Press, Cambridge, 1990.

[16] O. Kesler, M. Finot, S. Suresh, S. Sampath, Determination of processing-induced stresses and properties of layered and graded coatings: experimental method and results for plasma-sprayed Ni–Al_2O_3, Acta Metall. Mater. 45 (8) (1997) 3123–3134.
[17] M. Koizumi, FGM activities in Japan, Composites Part B 28B (1997) 1–4.
[18] T. Mori, K. Tanaka, Average stress in matrix and average elastic energy of materials with misfitting inclusions, Acta Metall. 21 (1973) 571–574.
[19] J.T. Oden, G.F. Carey, Finite Elements: Computational Aspects, vol. III, Prentice-Hall, Englewood Cliffs, NJ, 1984.
[20] J.T. Oden, T. Zohdi, Analysis and adaptive modeling of highly heterogeneous elastic structures, Comput. Meth. Appl. Mech. Engrg. 148 (1997) 367–391.
[21] K.S. Ravichandran, Elastic properties of two-phase composites, J. Am. Ceram. Soc. 77 (5) (1994) 1178–1184.
[22] T. Reiter, G.J. Dvorak, V. Tvergaard, Micromechanical models for graded composite materials, J. Phys. Solids 45 (1997) 1281–1302.
[23] T. Reiter, G.J. Dvorak, Micromechanical models for graded composite materials: II. Thermomechanical loading, J. Phys. Solids 46 (9) (1998) 1655–1673.
[24] R.A. Schapery, Thermal expansion coefficients of composite materials, J. Comput. Mater. 2 (1968) 380–404.
[25] S. Suresh, A.E. Giannakopoulos, M. Olson, Elastoplastic analysis of thermal cycling: layered materials with sharp interfaces, J. Mech. Phys. Solids 42 (6) (1994) 978–1018.
[26] M. Takemura, A. Yoshitake, H. Hayakawa, T. Hyakubu, M. Tamura, Mechanical and thermal properties of FGM fabricated by thin lamination method, in: Proceedings of the First International Symposium on Functionally Gradient Materials Forum, 1990, pp. 97–100.
[27] Y. Tomota, K. Kuroki, T. Mori, I. Tamura, Tensile deformation of two-ductile-phase alloys: flow curves of $\alpha - \gamma$ Fe–Cr–Ni alloys, Mater. Sci. Engrg. 24 (1976) 85–94.
[28] K. Wakashima, H. Tsukamoto, Mean-field micromechanics model and its application to the analysis of thermomechanical behavior of composite materials, Mater. Sci. Engrg. A 146 (1991) 291–316.
[29] K. Wakashima, H. Tsukamoto, A unified micromechanical approach toward thermomechanical tailoring of metal matrix composites, ISIJ Int. 32 (8) (1992) 883–892.
[30] L.J. Walpole, On the bounds for the overall elastic moduli of inhomogeneous systems, J. Mech. Phys. Solids 14 (1966) 151–162.
[31] E. Weissenbek, H.E. Pettermann, S. Suresh, Elasto-plastic deformation of compositionally graded metal–ceramic composites, Acta Mater. 45 (8) (1997) 3401–3417.
[32] R.L. Williamson, B.H. Rabin, J.T. Drake, Finite element analysis of thermal residual stresses at graded ceramic–metal interfaces, Part 1, Model description and geometrical effects, J. Appl. Phys. 74 (2) (1993) 1310–1320.
[33] A. Yoshitake, M. Tamura, I. Shito, M. Niino, Fabrication of the functionally gradient materials (FGM), In: The State of Art, ESA Symposium on Space Applications of Advanced Structural Materials, 1990.